Transmembrane peptides

DOI: 10.1002/anie.200705993

Effects of Guanidinium–Phosphate Hydrogen Bonding on the Membrane-Bound Structure and Activity of an Arginine-Rich Membrane Peptide from Solid-State NMR Spectroscopy

*Ming Tang, Alan J. Waring, Robert I. Lehrer, and Mei Hong**

Arginine- and lysine-rich cationic peptides and protein domains are found in a wide range of membrane-active proteins such as antimicrobial peptides,[1] cell-penetrating peptides,[2] and voltage-sensing domains of potassium channels.[3] Yet the three-dimensional structures these proteins adopt to enable translocation of the charged residues into the low dielectric milieu of the hydrophobic part of the lipid membrane, despite the free-energy barrier,[4] remain poorly understood. An increasing number of molecular dynamics simulations and experimental studies have suggested the importance of Arg interactions with lipids in membrane protein function.[5,6] Magic-angle spinning (MAS) solid-state NMR (SSNMR) spectroscopy can provide direct experimental insights into these intriguing questions of energetics and structure.

We have recently reported SSNMR distance-constrained guanidinium–phosphate ($Gdn–PO_4^-$) complex formation between the Arg residues of a β-hairpin antimicrobial peptide, PG-1, and the lipid phosphate groups.[7] The existence of these complexes suggests that the Arg residues are neutralized by the phosphate groups to enable transmembrane insertion of the peptide. We hypothesized that the peptide-associated phosphate headgroups transferred to the hydrophobic part of the membrane are responsible for the toroidal pore defects.[8] Such $Gdn–PO_4^-$ complexes should be stabilized by N–H···O=P hydrogen bonds and electrostatic attractions.[9]

Herein we test the importance of $Gdn–PO_4^-$ hydrogen bonding to the structure and activity of PG-1 by dimethylating each guanidinium group, thus reducing the number of N–H hydrogen-bond donors (Figure 1).[10] We show that this dimethylation of the Arg groups significantly alters the membrane insertion and activity of PG-1. Figure 2 shows oriented ^{31}P NMR spectra of palmitoyloleoylphosphatidylcholine/palmitoyloleoylphosphatidylglycerol (POPC/POPG) membranes containing 0–4% of the mutant (Arg^{mm}-PG-1).

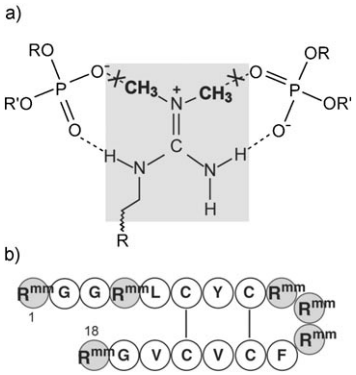

Figure 1. a) Structure of dimethylated Arg residue and its bidentate complex with phosphate ions. b) Arg^{mm}-PG-1 amino acid sequence.

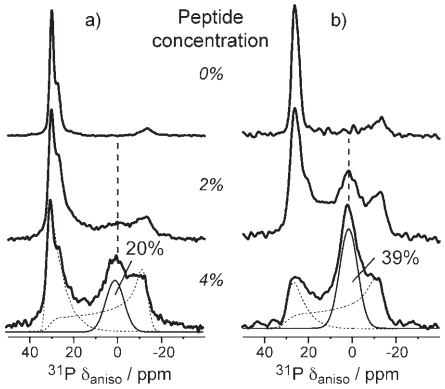

Figure 2. Oriented ^{31}P NMR spectra of POPC/POPG membranes with 0–4% a) Arg^{mm}-PG-1 and b) PG-1. The 4% sample spectra are simulated with an aligned peak, an isotropic peak, and a powder pattern, to yield the fraction of the isotropic peak.

Without the peptide, the membranes uniaxially aligned on glass plates and exhibited the expected single peak at approximately 30 ppm without other intensities in the anisotropic chemical shift range. Residual powder intensities indicative of misalignment and a small 0 ppm isotropic peak indicative of toroidal pores are observed with increasing concentrations of Arg^{mm}-PG-1. Line-shape simulations indicate that the isotropic component in the 4% Arg^{mm}-PG-1 sample is 20% of the total intensity, much less than the 39% caused by PG-1; thus, dimethylation of the Arg residues reduces membrane disruption.

Corroborating the ^{31}P NMR data are the minimal effective concentrations (MECs) of Arg^{mm}-PG-1 and PG-1 against

[*] M. Tang, Dr. M. Hong
Department of Chemistry, Iowa State University
Ames, IA 50011 (USA)
Fax: (+1) 515-294-0105
E-mail: mhong@iastate.edu
Homepage: http://www.public.iastate.edu/~hongweb
Dr. A. J. Waring, Dr. R. I. Lehrer
Department of Medicine
University of California at Los Angeles
Los Angeles, CA 90095 (USA)

Supporting information for this article is available on the WWW under http://www.angewandte.org or from the author.

a number of bacteria. In a solution containing salt concentrations similar to physiological levels, the average MEC of Arg^{mm}-PG-1 is 3.4-fold higher than PG-1, indicating that the mutant is 3.4-fold less potent (see the Supporting Information Table S1). At low salt concentration Arg^{mm}-PG-1 is still 1.4-fold less potent than PG-1. The weaker activity supports the lower membrane disorder of Arg^{mm}-PG-1 observed in the ^{31}P NMR spectra. The salt-concentration dependence of the two peptides suggests different mechanisms are involved in their antimicrobial action (see the Supporting Information).

To determine the topological structure of Arg^{mm}-PG-1 in the lipid membrane we measured the peptide–lipid ^{13}C–^{31}P distances. Figure 3 shows rotational echo double resonance (REDOR) distance curves of several ^{13}C-labeled sites. The Cα atom of L5, which is next to the most hydrophobic Arg residue, R4, increased its distance from 6.9 ± 1.6 Å in PG-1 to 8.5 Å in Arg^{mm}-PG-1, suggesting that the R4 mutation weakened the Gdn–PO_4^- complex. All measured distances are within 5.7–8.5 Å. Since the membrane has fewer isotropic defects in the presence of Arg^{mm}-PG-1 the distance similarity suggests that Arg^{mm}-PG-1 binds at the membrane/water interface, and the strand axis is roughly parallel to the membrane plane.

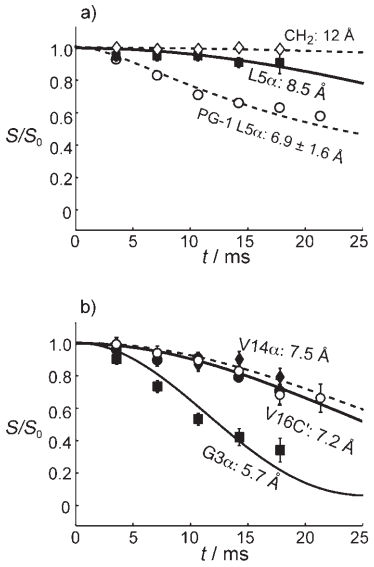

Figure 3. ^{13}C–^{31}P NMR distances of Arg^{mm}-PG-1 in hydrated POPE/POPG membranes. a) L5α (■) in Arg^{mm}-PG-1, compared with PG-1 (○). Lipid CH_2 data (◇) give the long distance limit. b) G3α (■) and V14α (◆) in Arg^{mm}-PG-1, and V16C′ in Arg^{mm}-PG-1 (●) and in PG-1 (○). S/S_0 is the intensity ratio of the REDOR dephasing spectrum with the control spectrum, measured with the ^{31}P pulses on and off, respectively.

We measured the distance between Arg^{mm}-PG-1 and the lipid chains by using a two-dimensional ^{31}P-detected ^1H spin diffusion experiment to verify the interfacial hypothesis.[11] In a peptide-free membrane the lipid chain $(CH_2)_n$ cross peak with the ^{31}P NMR signal is very weak because of the long distance and high mobility of the lipids. A rigid transmembrane (TM) peptide facilitates spin diffusion by its strongly coupled ^1H network, giving a high CH_2–P intensity. In contrast, a surface-bound peptide or a TM peptide with large-amplitude motion is an ineffective spin-diffusion conduit and produces low CH_2–P intensities.

The two-dimensional spectrum of Arg^{mm}-PG-1 in the POPE/POPG membrane at a mixing time of 64 ms is shown in Figure 4a. In the one-demensional cross sections the Arg^{mm}-PG-1 CH_2 intensity is higher than that of the pure membrane and lower than that of PG-1 (Figure 4b–d). The CH_2 build-up curves (Figure 4e) confirm that PG-1 has the fastest increase in intensity, as expected for the TM peptide; Arg^{mm}-PG-1 has a slower increase in intensity for the build-up curve, and the peptide-free bilayer has the smallest slope. These data support the interfacial binding of Arg^{mm}-PG-1.

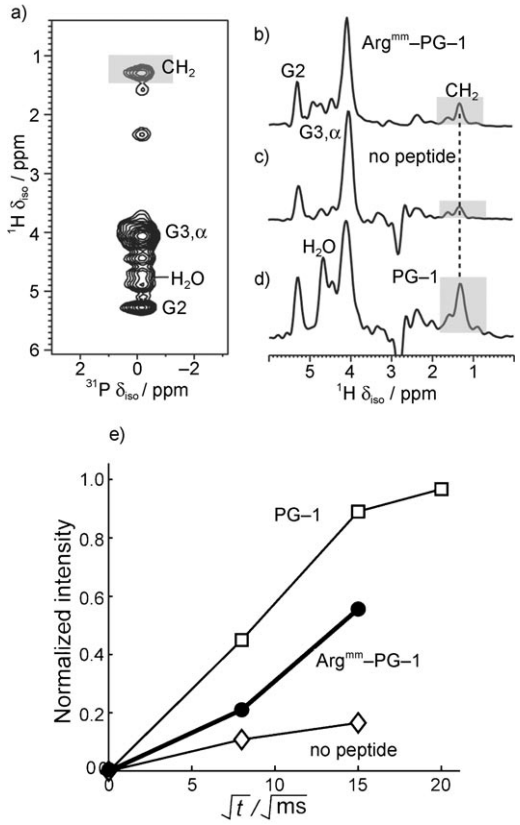

Figure 4. ^{31}P-detected ^1H spin diffusion spectra of POPE/POPG membranes at 303 K. a) 64 ms two-dimensional spectrum of Arg^{mm}-PG-1-containing membrane. b–d) 64 ms one-dimensional cross sections of membranes containing b) Arg^{mm}-PG-1, c) no peptide, and d) PG-1. e) CH_2 build-up curves for the three samples.

If Arg^{mm}-PG-1 is a TM peptide but highly mobile, it could still satisfy the ^1H spin diffusion data, therefore we measured C–H dipolar couplings of two Cα sites. Both L5 and V14 give Cα–Hα couplings that are 60–70% of the rigid-limit value in the POPC/POPG membrane (Table 1; and shown in two-dimensional Lee–Goldburg cross-polarization (LG-CP)[12] spectra in the Supporting Information, Figure S1), indicating that the peptide is mobile. This mobility contrasts with the fully immobilized PG-1 backbone in anionic membranes.[13,14] L5 and V14 are located next to disulfide bonds, thus backbone

Table 1: Cα $S_{Cα\text{-}Hα}$ values of Arg^{mm}-PG-1 in two anionic lipid membranes.

$S_{Cα\text{-}Hα}$	POPC/POPG	POPE/POPG
L5	0.69	0.84
V14	0.62	0.37

segmental motion is unlikely, and the reduced couplings are most likely because of rigid-body rotation of Arg^{mm}-PG-1 around the bilayer normal ($\vec{n}$). Indeed, recoupled Cα chemical shift anisotropies (CSA) of L5 and V14 show uniaxial line shapes (see the Supporting Information, Figure S2), confirming the uniaxiality of the backbone motion. Under this rotation, the $S_{Cα\text{-}Hα}$ value depends on the C–H bond orientation with respect to $\vec{n}$ as $S_{CH} = \langle(3\cos^2\theta - 1)/2\rangle$; the L5 and V14 $S_{Cα\text{-}Hα}$ values must be related by the orientations of the two bonds to each other and to $\vec{n}$, and therefore $S_{Cα\text{-}Hα}$ should indicate the peptide orientation.[15,16]

Calculated $S_{Cα\text{-}Hα}$ values for strand residues in an ideal antiparallel β-hairpin as a function of (τ, ρ) angles are shown (Figure 5 and the Supporting Information, S3 and S4):[17] τ is the tilt angle between the strand axis and $\vec{n}$ and ρ is the

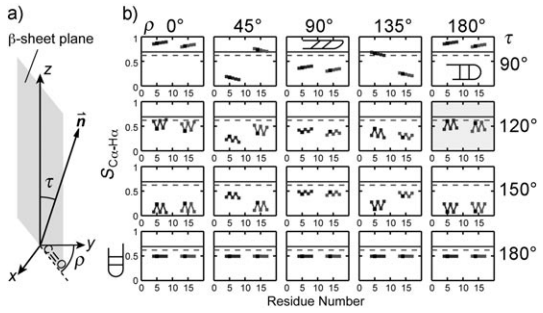

Figure 5. a) Definition of (τ, ρ) angles. τ is the angle between the strand axis *z* and the bilayer normal $\vec{n}$, and ρ is the angle between the C=O bond of residue six and the common plane of *z* and $\vec{n}$. b) Calculated $S_{Cα\text{-}Hα}$ of the strand residues (4–8 and 13–17) in an ideal β-hairpin as a function of (τ, ρ). The measured $S_{Cα\text{-}Hα}$ of L5 and V14 are drawn as solid and dashed lines, respectively. The best-fit (τ, ρ) panel, near (120°, 180°), is shaded.

rotation angle of the β-hairpin plane from $\vec{n}$. $\rho = 0°$ when $\vec{n}$ lies in the β-sheet plane. For the TM case $\tau \approx 180°$ and the $S_{Cα\text{-}Hα}$ value is generally less than 0.5 because the Cα–Hα bonds are close to being perpendicular to $\vec{n}$. For τ values of 130–180°, the calculated S_{CH} value is less than 0.6 for L5 and V14, which is inconsistent with the experimental data. As the strands become more parallel to the bilayer plane ($\tau \rightarrow 90°$), $S_{Cα\text{-}Hα}$ values become larger and vary over the entire range of 0–1. The best fit is when $\tau = 116°$ and $\rho = 179°$, indicating that the strand axis is roughly orthogonal to $\vec{n}$ and the hairpin plane is parallel to $\vec{n}$. The latter is reasonable because the peptide meets the least resistance in this orientation as it inserts into the membrane. Three other symmetry-related (τ, ρ) solutions exist, but they agree less well with the ^{13}C–^{31}P NMR distance data (see the Supporting Information, Table S2).

If residual segmental motion had remained at L5 and V14 Cα, it would mean that the whole-body $S_{Cα\text{-}Hα}$ value would be larger than 0.6–0.7, which would require τ to be even closer to 90°. Thus, the strand axis must be parallel to the membrane plane. In the POPE/POPG membrane, the L5 and V14 $S_{Cα\text{-}Hα}$ values change to 0.84 and 0.37, respectively (Table 1). The difference translates to only small (τ, ρ) changes, because of the high angular resolution of $S_{Cα\text{-}Hα}$ in this regime (see the Supporting Information, Figure S5), and the best fit is for τ at 113° and ρ at 164°. Thus, Arg^{mm}-PG-1 is interfacial in both anionic membranes. We also considered the effect of the backbone structure on the orientation calculation; the data show that even with the non-ideal PG-1 solution structure, the C–H dipolar couplings still constrain the strand axis to be perpendicular to $\vec{n}$ (see the Supporting Information, Figure S6 and Table S2).

Figure 6 summarizes the dramatic topology difference of Arg^{mm}-PG-1 and PG-1 in the lipid membrane. Compared to PG-1, the hydrogen bond deficient mutant is no longer a TM

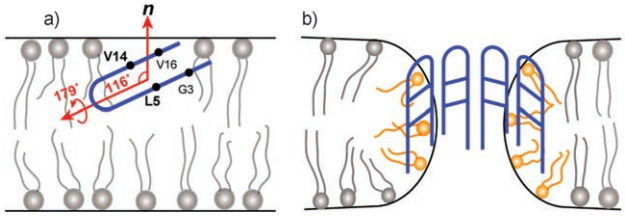

Figure 6. Topological structure of a) Arg^{mm}-PG-1 and b) PG-1 in anionic lipid membranes.

peptide, but is inserted to the membrane/water interface, 5.7–8.5 Å from the ^{31}P plane and further from the hydrophobic center of the membrane. The mutant is uniaxially mobile and thus not oligomerized, whereas PG-1 forms immobile multimeric β-barrels in the anionic membrane, possibly promoted by a high salt concentration. Thus, the reduction of hydrogen bonds caused by the dimethylation of the Arg residues in this antimicrobial peptide weakens Gdn–PO_4^- complexation, prevents peptide insertion and oligomerization, and reduces the disruptive activity of the peptide to the membrane. The data herein suggest that the remaining activity of Arg^{mm}-PG-1 is achieved by a different mechanism, most likely in-plane diffusion, which still gives rise to isotropic lipid morphologies, albeit at a lower level than the toroidal pore mechanism employed by wild-type PG-1.[18] Gdn–PO_4^- hydrogen bonding may also affect the structure and function of other Arg-rich membrane proteins, as suggested by recent molecular dynamics simulations of a potassium channel and a cell-penetrating peptide.[3,5,6]

Experimental Section

Arg^{mm}-PG-1 is synthesized by Fmoc chemistry and purified to greater than 95%. The peptides were reconstituted into lipid vesicles at a peptide/lipid molar ratio of 1:15. All NMR data were obtained at 9.4 Tesla by using a triple-resonance 4 mm MAS probe and a static probe. ^{13}C–^{31}P NMR REDOR experiments were conducted at 225 K

under 4.5 kHz MAS. Two-dimensional LG-CP and DIPSHIFT experiments were used to measure C–H dipolar couplings and the ROCSA experiment was used to measure the ^{13}C NMR CSA values. Further details of orientation simulations are given in the Supporting Information.

Received: December 30, 2007
Revised: February 12, 2008
Published online: March 13, 2008

Keywords: guanidinium ions · NMR spectroscopy · phospholipids · proteins · structure elucidation

[1] M. Zasloff, *Nature* **2002**, *415*, 389.
[2] R. Fischer, M. Fotin-Mleczek, H. Hufnagel, R. Brock, *ChemBioChem* **2005**, *6*, 2126.
[3] Y. Jiang, V. Ruta, J. Chen, A. Lee, R. MacKinnon, *Nature* **2003**, *423*, 42.
[4] T. Hessa, H. Kim, K. Bihlmaier, C. Lundin, J. Boekel, H. Andersson, I. Nilsson, S. H. White, G. von Heijne, *Nature* **2005**, *433*, 377.
[5] J. A. Freites, D. J. Tobias, G. von Heijne, S. H. White, *Proc. Natl. Acad. Sci. USA* **2005**, *102*, 15059.
[6] H. D. Herce, A. E. Garcia, *Proc. Natl. Acad. Sci. USA* **2007**, *104*, 20805.
[7] M. Tang, A. J. Waring, M. Hong, *J. Am. Chem. Soc.* **2007**, *129*, 11438.
[8] K. Matsuzaki, O. Murase, N. Fujii, K. Miyajima, *Biochemistry* **1996**, *35*, 11361.
[9] K. A. Schug, W. Lindner, *Chem. Rev.* **2005**, *105*, 67.
[10] J. B. Rothbard, T. C. Jessop, R. S. Lewis, B. A. Murray, P. A. Wender, *J. Am. Chem. Soc.* **2004**, *126*, 9506.
[11] D. Huster, X. L. Yao, M. Hong, *J. Am. Chem. Soc.* **2002**, *124*, 874.
[12] B. J. vanRossum, C. P. deGroot, V. Ladizhansky, S. Vega, H. J. M. deGroot, *J. Am. Chem. Soc.* **2000**, *122*, 3465.
[13] J. J. Buffy, A. J. Waring, R. I. Lehrer, M. Hong, *Biochemistry* **2003**, *42*, 13725.
[14] R. Mani, S. D. Cady, M. Tang, A. J. Waring, R. I. Lehrer, M. Hong, *Proc. Natl. Acad. Sci. USA* **2006**, *103*, 16242.
[15] M. Hong, T. Doherty, *Chem. Phys. Lett.* **2006**, *432*, 296.
[16] S. D. Cady, C. Goodman, C. Tatko, W. F. DeGrado, M. Hong, *J. Am. Chem. Soc.* **2007**, *129*, 5719.
[17] M. Tang, A. J. Waring, R. I. Lehrer, M. Hong, *Biophys. J.* **2006**, *90*, 3616.
[18] T. Doherty, A. J. Waring, M. Hong, *Biochemistry* **2008**, *47*, 1105.

Angewandte Chemie
Eine Zeitschrift der Gesellschaft Deutscher Chemiker

Supporting Information

69451 Weinheim, Germany

Supporting Information

Effects of Guanidinium-Phosphate Hydrogen Bonding on the Membrane-Bound Structure and Activity of an Arginine-Rich Membrane Peptide from Solid-State NMR

Ming Tang[1], Alan J. Waring[2], Robert I. Lehrer[2], and [1]

[1.] Department of Chemistry, Iowa State University, Ames, IA 50011

[2] Department of Medicine, University of California at Los Angeles, Los Angeles, CA 90095

Antimicrobial assays

Radial diffusion assays were performed in media supplemented with 100 mM NaCl or in low salt media. Both assay media contained 10 mM sodium phosphate buffer, 1% agarose, and 0.3 mg/ml of trypticase soy broth powder to allow the organisms to grow until the underlay assay gel was covered with a nutrient-rich overlay gel that allowed surviving microbes to form colonies. The high-salt results are more predictive of activity in physiological fluids.

Table S1. Minimum effective concentrations (MEC) of PG-1 and Arg^{mm}-PG-1 against various bacteria at high and low salt conditions.

MEC (μg/ml)	100 mM NaCl		Low NaCl	
	PG-1	Arg^{mm}-PG-1	PG-1	Arg^{mm}-PG-1
Gram-negative bacteria				
E. coli	1.09	3.00	1.55	1.58
P. aeruginosa	1.39	3.41	1.90	1.62
K. pneumoniae	1.93	8.76	4.47	7.9
Gram-positive bacteria				
S. epidermidis	1.07	1.90	4.19	4.29
E. faecalis	1.54	3.10	4.10	3.17
B. subtilis	1.22	3.91	1.79	3.58
S. aureus	1.66	10.4	5.10	9.35
mean (n=7)	**1.41**	**4.92**	**3.30**	**4.50**

The mean activities of PG-1 and Arg^{mm}-PG-1 in 100 mM NaCl differ significantly ($p<0.001$ by the Mann-Whitney Rank Sum test).

Table 1 shows that higher salt concentration increases the activity of PG-1, but does not affect the activity of Arg^{mm}-PG-1. We hypothesize that higher salt concentration promotes PG-1 aggregation, which is essential for its toroidal-pore mechanism of action [2]. In our previous study of the structure of PG-1 fibrils outside the lipid membrane,[1]

high salt concentration was used to promote fibril formation. The fact that salt level does not affect the activity of Arg^{mm}-PG-1 suggests that the mutant adopts a different mechanism of action that does not require peptide aggregation. This is consistent with the large-amplitude dynamics observed for the mutant.

Motionally averaged dipolar couplings and chemical shift anisotropies

C-H dipolar couplings of Arg^{mm}-PG-1 were measured using the 2D LG-CP experiment [3] for the POPC/POPG sample and the DIPSHIFT experiment [4] for the POPE/POPG sample. The LG-CP experiment was conducted under 10 kHz spinning at 295 K. The DIPSHIFT experiment was performed under 3.5 kHz MAS at 303 K, the higher temperature due to the higher phase transition temperature of the POPE/POPG membrane. The MREV-8 sequence was used for ^{1}H homonuclear decoupling. The scaling factors for the LG-CP sequence and the MREV-8 sequence are 0.57 and 0.47, respectively.

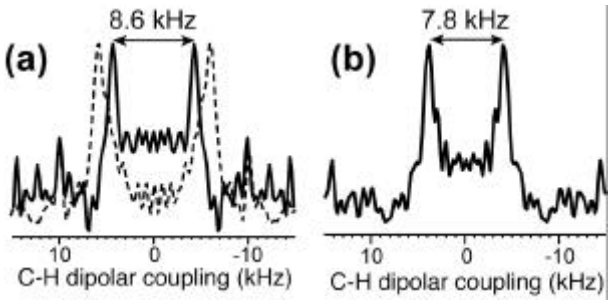

Fig. S1. ^{13}C-^{1}H LG-CP cross sections of Arg^{mm}-PG-1 in the POPC/POPG membrane at 295 K. (a) L5 Cα. (b) V14 Cα. Dashed line in (a) indicates the rigid-limit coupling of 12.5 kHz, measured at 233 K. The experimental uncertainty is ±0.2 kHz.

In addition to C-H dipolar couplings, we measured the Cα chemical shift anisotropy (CSA) of L5 and V14 using the ROCSA experiment [5] to assess if the backbone motion is uniaxial. The experiment was carried out at 303 K on the POPE/POPG membrane samples under 6 kHz MAS. Fig. S2 shows the ROCSA spectra and the relevant peptide and lipid cross sections. The lipid cross sections (Fig. S2c) give a control of the expected uniaxial lineshapes due to the known uniaxial rotation of lipids around the bilayer normal. It can be seen that the peptide L5 and V14 Cα sites also have uniaxial lineshapes (Fig. S2b), with motionally narrowed anisotropy parameter $\bar{\delta}$ of 17 ppm for L5 and 11 ppm for V14. The rigid-limit anisotropy parameter δ for β-sheet Val is known from previous experimental studies to be 25 ppm [6], while the rigid-limit δ for the β-sheet conformation of Leu has been obtained from *ab initio* calculations to be 19.5 ppm [7]. Thus, the CSA order parameter $S_{CSA} = \bar{\delta}/\delta$ is 0.89 for L5 and 0.44 for V14. These values are consistent with the C-H order parameters measured for these two sites in the POPE/POPG membrane. Most importantly, the uniaxial CSA lineshapes confirm the presence of uniaxial rotation of the Arg^{mm}-PG-1 backbone around the membrane normal.

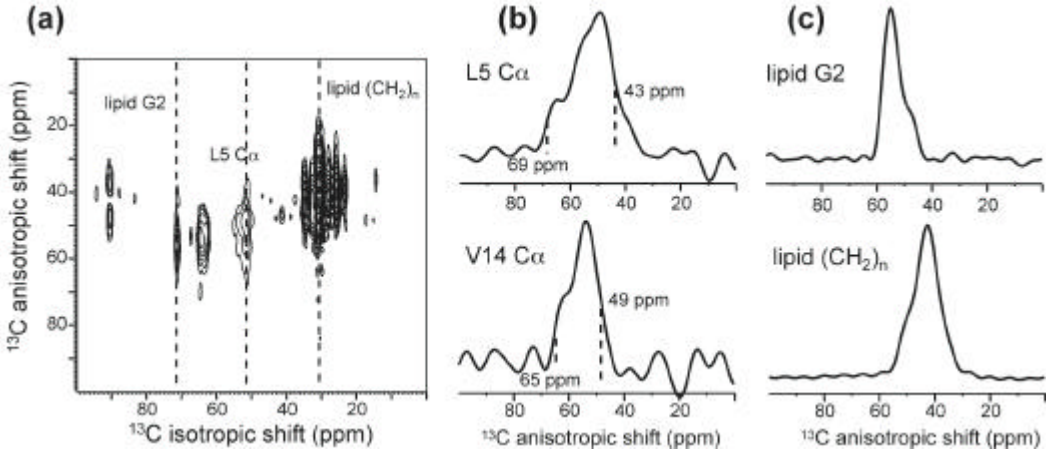

Fig. S2. $^{13}C\alpha$ CSA of Arg^{mm}-PG-1. (a) 2D ROCSA spectra of Arg^{mm}-PG-1 in POPE/POPG membranes at 303 K. (b) 1D cross sections of the peptide L5 and V14 Cα sites. (c) 1D cross sections of two lipid peaks, glycerol G2 and acyl chain $(CH_2)_n$. The lipid lineshapes are uniaxial as expected. The peptide lineshapes are similarly uniaxial, indicating uniaxial rotation around the membrane normal.

Orientation calculations

The ideal antiparallel β-hairpin structure was constructed using (ϕ, ψ) torsion angles of (-137°, +135°) for the strand residues, and (-45°, +85°) and (+155°, -20°) for the *i*+1 and *i*+2 residues of the β-turn [8]. The turn torsion angles were modified from the classical β-turn conformations to make the two strands approximately parallel. The strand axis was chosen to be the average orientation of six consecutive C'-N bonds from residue 4 to residue 9. The tilt angle τ is the angle between this strand axis and the bilayer normal. The ρ angle was defined as the angle between the C=O bond of residue 6 and the common plane of the strand axis and the bilayer normal. The peptide was rotated through all combinations of (τ, ρ) angles and the C-H dipolar couplings of the N-strand residues 4 - 8 and C-strand residues 13 - 17 were calculated and converted to the order parameter according to $S_{CH} = \omega(\tau,\rho)/\omega_{rigid}$.

Fig. S3 shows a more extended set of S_{CH} values for (τ, ρ) angles in the range (10-90°, 0°-180°), which complements the simulations in Fig. 5. The best fit (τ, ρ) in this range for the POPC/POPG bound Arg^{mm}-PG-1 is (64°, 359°), and is related to the global best fit (116°, 179°) by symmetry.

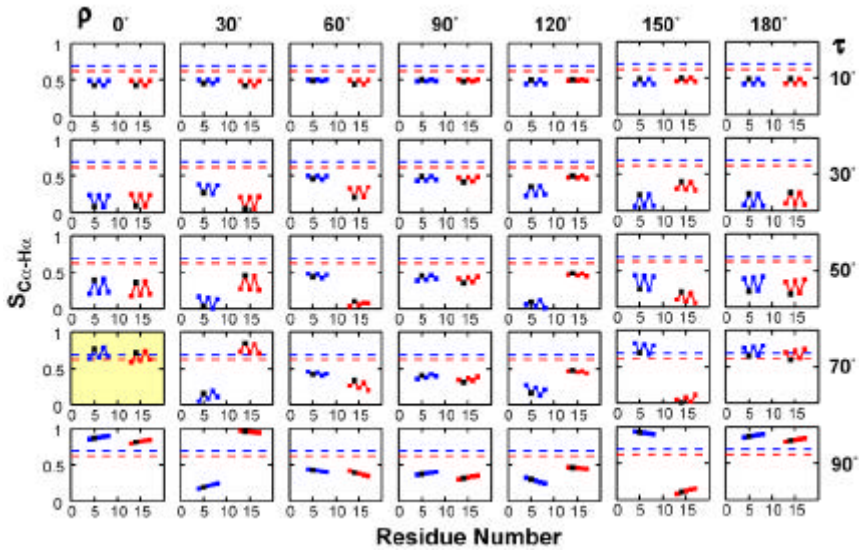

Fig. S3. S_{CH} of an ideal β-hairpin as a function of (τ, ρ). The N- and C-strand S_{CH}'s are plotted as blue and red squares, respectively, with the L5 and V14 values in black. The experimental S_{CH}'s for L5 and V14 in the POPC/POPG membrane are drawn as blue and red dashed lines. The yellow highlighted panel indicates the approximate position of one of the four best-fit orientations.

Fig. S4 shows the RMSD between the calculated S_{CH} and the experimental S_{CH}'s of L5 and V14 in the POPC/POPG membrane. The RMSD is calculated as

$$\text{RMSD} = \sqrt{\left(S_{CH,calc}^{L5} - S_{CH,exp\,t}^{L5}\right)^2 + \left(S_{CH,calc}^{V14} - S_{CH,exp\,t}^{V14}\right)^2}.$$

From the RMSD, four symmetry-related best-fit orientations are identified and listed in Table S2. Taking into account the ^{13}C-^{31}P distance constraints, the global best-fit (τ, ρ) angles are orientation A, (116°, 179°).

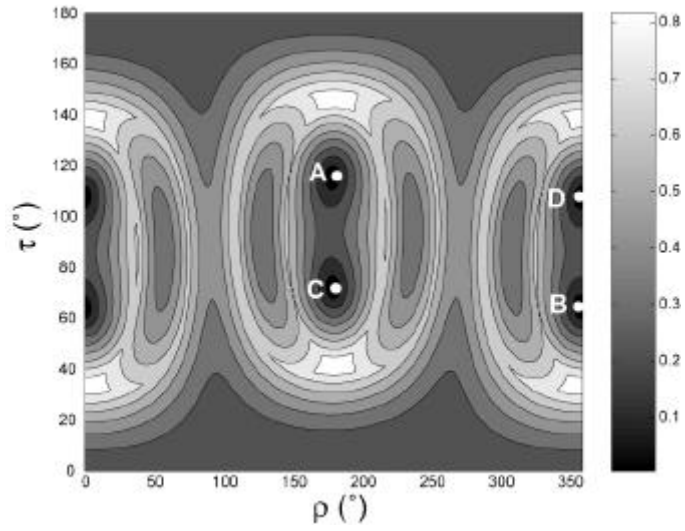

Fig. S4. RMSD between the calculated and experimental Cα-Hα order parameters of Arg^{mm}-PG-1 in the POPC/POPG membrane as a function of (τ, ρ). The four lowest RMSD positions are related by symmetry and are indicated as A, B, C, D.

To obtain the peptide orientation in the POPE/POPG membrane, we carried out the same S_{CH} calculation but compared these with the POPE/POPG experimental data. Fig. S5a shows S_{CH} for (τ, ρ) of (50-130°, 160°-340°). The ideal β-hairpin structure is used in the calculation. Again, four symmetry-related best-fit orientations are found according to the RMSD analysis (Fig. S5b). The orientation (τ, ρ) = (113°, 164°) is chosen as the global best fit because it agrees best with the ^{13}C-^{31}P distance data. This orientation is quite similar to that found in POPC/POPG membranes, as shown by the schematic representation in Fig. S5c, indicating that the composition change from POPC to POPE lipids does not affect the Arg^{mm}-PG-1 orientation significantly.

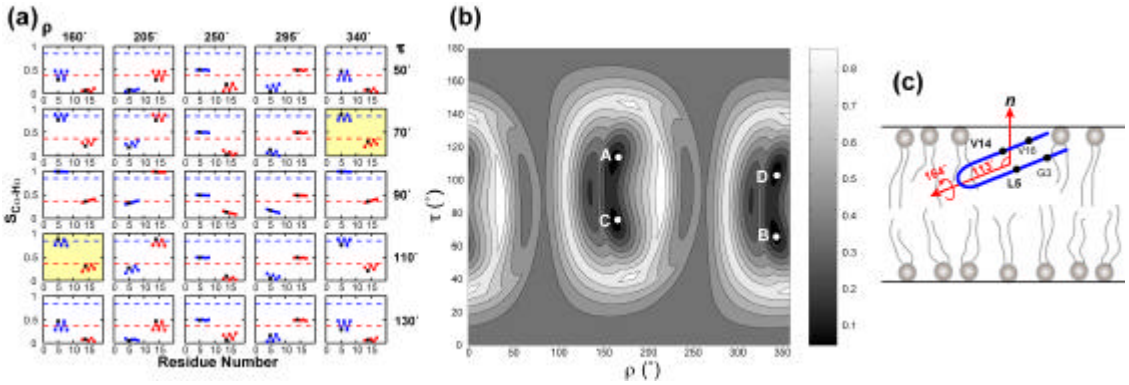

Fig. S5. Orientation of Arg^{mm}-PG-1 in the POPE/POPG membrane. (a) S_{CH} of an ideal β-hairpin for various (τ, ρ) angles. The N- and C-strand S_{CH}'s are plotted as blue and red squares, respectively, with L5 and V14 values in black. The experimental Cα S_{CH}'s for L5 and V14 in the POPE/POPG membrane are drawn as blue and red dashed lines, respectively. Some of the approximate best-fit orientations are highlighted in yellow to indicate the agreement with the experimental data. (b) RMSD between the calculated and experimental Cα-Hα order parameters of Arg^{mm}-PG-1 in the POPE/POPG membrane as a function of (τ, ρ). (c) Topological structure of Arg^{mm}-PG-1 in the POPE/POPG membrane.

To assess if the structure used in the S_{CH} calculation affects the orientation result significantly, we also calculated S_{CH} using the solution NMR structure of PG-1 (PDB: 1PG1) [9]. In the 20 energy-minimized structures, the backbone conformations of the β-strand residues 5-9 and 12-17 have relatively small variations. We chose the representative structure #10 as the input for the orientation calculation. Fig. S6 shows that the best-fit τ angles fall in the same range as the ideal hairpin simulations, close to 90°, thus the conclusion that the strand axis is roughly parallel to the membrane plane is

unchanged. However, for the POPC/POPG membrane, even the best-fit (τ, ρ) angles of (100°, 152°) does not agree with the experimental data very well (Fig. S6a), suggesting that the solution structure of PG-1 may deviate non-negligibly from the membrane-bound peptide structure. Nevertheless, the best-fit (τ, ρ) range of (60°-90°, 150°-180°) is in general good agreement with the ideal hairpin simulations (Table S2). In conclusion, Arg^{mm}-PG-1 has the strand axis perpendicular to the membrane normal and has the hairpin plane roughly parallel to the membrane normal, regardless of the input structure.

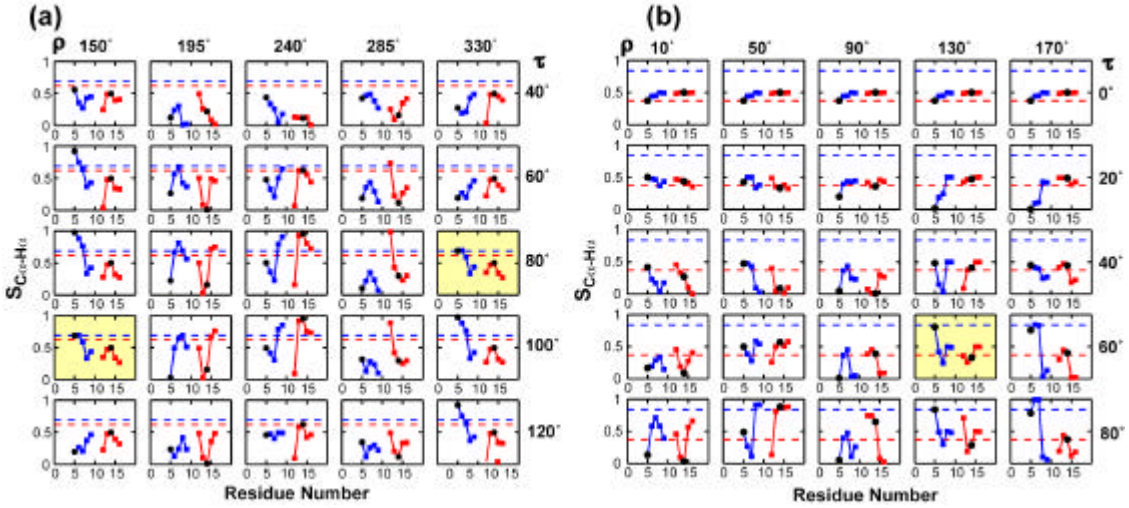

Fig. S6. Calculated S_{CH}'s using the PG-1 solution structure #10. Values of residues 5-9 and 12-17 are shown in blue and red squares, respectively, with the L5 and V14 S_{CH}'s in black. The experimental S_{CH}'s for L5 and V14 are drawn as blue and red dashed lines, respectively. (a) Experimental data is that of the POPC/POPG membrane. (b) Experimental data is that of the POPE/POPG membrane. The approximate best-fit orientations are highlighted in yellow to indicate the agreement with the experimental data.

The somewhat different quality of fit between the PG-1 solution NMR structure and the ideal β-hairpin structure can be explained by the distorted backbone conformation of the PG-1 solution structure, shown in Fig. S7. The Cα-Hα vectors are along the same direction in the ideal β-hairpin, but point to a range of directions in the solution NMR structure #10.

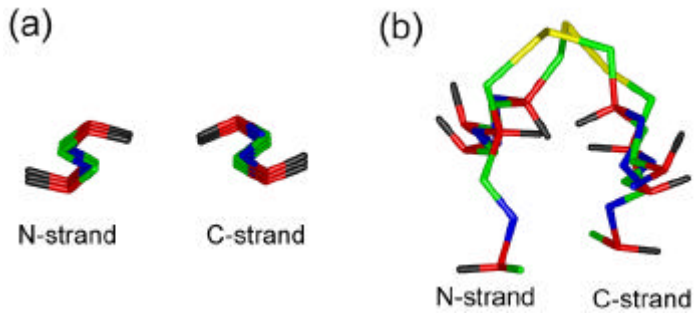

Fig. S7. Comparison of the structures of (a) the ideal β-hairpin and (b) PG-1 solution NMR structure #10 (PDB: 1PG1). Cα and Hα atoms are highlighted in red and black, respectively. The β-strand axis is perpendicular to the view plane. Residues 5-9 and 12-17 are shown in sticks.

Table S2 summarizes the best-fit orientations of Arg^{mm}-PG-1 in POPC/POPG and POPE/POPG membranes from simulations using the ideal β-hairpin structure and the solution NMR structure #10. The global best-fit angles in each case after taking into account the ^{13}C-^{31}P distance constraints is listed in column A. All global best-fit orientations fall into a relatively narrow range of (τ, ρ) = (85-120°, 130-180°), indicating that Arg^{mm}-PG-1 strand axis is perpendicular to the bilayer normal. This is distinctively different from the transmembrane orientation of PG-1 [2].

Table S2. Best-fit (τ, ρ) angles for Arg^{mm}-PG-1 in POPC/POPG and POPE/POPG membranes. Solution A is the global best-fit based on agreement with the ^{13}C-^{31}P distance constraints.

Structure	Membrane	**A**	B	C	D	Error
Ideal hairpin	POPC/POPG	**(116°, 179°)**	(64°, 359°)	(72°, 179°)	(108°, 359°)	± 3°
Ideal hairpin	POPE/POPG	**(113°, 164°)**	(67°, 344°)	(76°, 164°)	(104°, 344°)	± 3°
PG-1 #10	POPC/POPG	**(100°, 152°)**	(80°, 332°)	(46°, 153°)	(134°, 333°)	—
PG-1 #10	POPE/POPG	**(89°, 137°)**	(91°, 317°)	(60°, 133°)	(120°, 313°)	± 6°

^{1}H spin diffusion

2D ^{31}P-detected ^{1}H spin-diffusion experiments were conducted at 303 K under 5 kHz MAS. After ^{1}H evolution, a mixing time (t_m) of 64 – 400 ms was applied to transfer ^{1}H polarization from the mobile lipids and water to the final destination of lipid headgroup ^{31}P for detection. In the absence of transmembrane proteins, the lipid chain CH_2 to ^{31}P cross peak is very slow to develop due to the extremely weak dipolar coupling. The presence of transmembrane peptides significantly facilitates the spin diffusion via the pathway CH_2 –> peptide –> ^{31}P. To ensure that only the mobile lipid and water polarization served as the source of spin diffusion, we suppressed the rigid peptide polarization by a ^{1}H T_2 relaxation filter of 0.8 ms before ^{1}H chemical-shift evolution and spin diffusion.

^{13}C-^{31}P distance measurement

^{13}C-^{31}P distances were measured using the rotational-echo double resonance (REDOR) experiment. Composite 90°180°90° pulses were applied on the ^{31}P channel to

reduce the effect of flip angle errors and enhance the distance accuracy. At each REDOR mixing time (t_m), a control experiment (S_0) with the ^{31}P pulses off and a dephasing experiment (S) with the ^{31}P pulses on were carried out. The normalized dephasing, S/S_0, as a function of t_m gives the ^{13}C-^{31}P dipolar coupling. The ^{13}CO dephasing was corrected for the lipid natural-abundance CO contribution. The experiments were conducted under 4.5 kHz MAS at 225 K. ^{31}P 180° pulse lengths of 9 μs were used to achieve complete inversion of the broad ^{31}P resonance.

References

[1] M. Tang, A. J. Waring, M. Hong, *J Am Chem Soc* **2005**, *127*, 13919.
[2] R. Mani, S. D. Cady, M. Tang, A. J. Waring, R. I. Lehrer, M. Hong, *Proc. Natl. Acad. Sci. U.S.A.* **2006**, *103*, 16242.
[3] B. J. vanRossum, C. P. deGroot, V. Ladizhansky, S. Vega, H. J. M. deGroot, *J. Am. Chem. Soc.* **2000**, *122*, 3465.
[4] M. Munowitz, W. P. Aue, R. G. Griffin, *J. Chem. Phys.* **1982**, *77*, 1686.
[5] J. C. C. Chan, R. Tycko, *J. Chem. Phys.* **2003**, *118*, 8378.
[6] X. L. Yao, M. Hong, *J. Am. Chem. Soc.* **2002**, *124*, 2730.
[7] H. Sun, L. K. Sanders, E. Oldfield, *J. Am. Chem. Soc.* **2002**, *124*, 5486.
[8] M. Tang, A. J. Waring, R. I. Lehrer, M. Hong, *Biophys. J.* **2006**, *90*, 3616.
[9] R. L. Fahrner, T. Dieckmann, S. S. Harwig, R. I. Lehrer, D. Eisenberg, J. Feigon, *Chem. & Biol.* **1996**, *3*, 543.